Femtosecond Dynamics and Vibrational Coherence in Gas-Phase Ultraviolet Photodecomposition of $Cr(CO)_6$

S. A. Trushin,*,† W. Fuss,* W. E. Schmid, and K. L. Kompa

Max-Planck-Institut für Quantenoptik, D-85748 Garching, Germany

Received: September 26, 1997; In Final Form: December 22, 1997

The initial dynamics of single-photon UV decomposition of $Cr(CO)_6$ to $Cr(CO)_5$ and CO in the gas phase was investigated by using femtosecond weak pump pulses at 267 nm and delayed, intense ionizing probe pulses at 800 nm with time-of-flight detection of ions. The parent and all the fragment ions show different temporal behavior at delay times of <200 fs, indicating that the molecules already go through several different configurations during this short time interval. With longer delays the heavy ions disappear, but light fragment-ion signals from $Cr(CO)_n^+$, $n = 3-0$, exhibit coherent oscillations with a wavenumber of 96 cm^{-1}, which can be assigned to the $C_{ax}-Cr-C_{eq}$ bending vibration of the neutral precursor $Cr(CO)_5$. The coherent oscillations are damped with a time constant of 815 fs. Our observations support a photochemical mechanism of chromium hexacarbonyl photodecomposition, proposed by Burdett et al. (*Inorg. Chem.* **1978**, *17*, 147): $M(CO)_6$ ($^1A_{1g}$) → $M(CO)_6$ ($^1T_{1u}$) → $M(CO)_6$ (a^1T_{2u}) → $M(CO)_5$(C_{4v}, 1^1E) → $M(CO)_5$ (D_{3h}, $1^1E'$) → $M(CO)_5$ (C_{4v}, 1^1A_1). The first step is induced by the pump pulse, and the next steps we have found to take 23, 10, 20, and 40 fs, respectively. A ground-state product $M(CO)_5$ (C_{4v}, 1^1A_1) is produced within 100 fs and exhibits a coherent $C_{ax}-Cr-C_{eq}$ bending oscillation. Ionization of vibrationally hot $Cr(CO)_5$ followed by thermal dissociation and photodissociation of the $Cr(CO)_5^+$ ion transfers these oscillations to $Cr(CO)_n^+$, $n = 3-0$. We point out that a conical intersection of the Jahn−Teller kind between the $1^1E'$ and 1^1A_1 states of chromium pentacarbonyl in a trigonal bipyramid geometry provides a path for ultrafast internal conversion from an electronically excited state to the ground state and also for the excitation of coherent oscillations at the $C_{ax}-Cr-C_{eq}$ bending coordinate, corresponding to Berry pseudorotation.

1. Introduction

The metal hexacarbonyls $M(CO)_6$ (M = Cr, Mo, W) have been used for more than 20 years as model systems to study the transition-metal carbonyl photochemistry. Extensive information about previous photochemical studies of these compounds can be found elsewhere.[1,2] Only the most important facts relevant to our results are noted here. Multiphoton collisionless decomposition of gas-phase $M(CO)_6$ results in effective stripping of all the ligands up to the naked metal atom for laser radiation ranging from UV to infrared.[3−5] One-photon UV laser photolysis of gaseous $M(CO)_6$ proceeds through the sequential loss of several carbonyl groups, depending on the radiation wavelength. In a low-temperature matrix and in liquid solution, however, UV photolysis results in efficient loss of only a single CO ligand to form a pentacarbonyl intermediate. The lack of multiple CO ligand loss in the latter case was attributed to the efficient energy relaxation of the highly vibrationally excited metal pentacarbonyl intermediate in the condensed-phase environment.[6] It is now generally accepted that the initial step of single-photon UV photolysis of metal hexacarbonyls in the gas phase is photochemical elimination of a single CO ligand followed by thermal loss of additional ligands from the vibrationally hot unsaturated carbonyls. Femtosecond time-resolved UV−visible and UV−infrared transient-absorption measurements in solution reveal the formation of vibrationally hot $Cr(CO)_5$ in the electronic ground state within 300 fs (see discussion in ref 2). However, these studies have mainly been directed toward understanding the effect of the solvent on postdissociation processes (vibrational relaxation and solvation), and the exact mechanism of the initial photochemical elimination, especially its early temporal dynamics, is not well established yet. In particular, it is not clear whether electronically excited states of the product are involved in the process or whether it is directly produced on its ground-state surface.

Femtosecond time-resolved multiphoton-ionization spectroscopy has proved to be a powerful tool in studying real-time chemical-reaction dynamics.[7] It has been employed to study the early dynamics of $Mn_2(CO)_{10}$[8] and $Fe(CO)_5$[9] photodecomposition under molecular-beam conditions. Recently, some advantages of probing by ionization, in particular under conditions of barrier suppression, have been demonstrated.[10] In this case ionization is assumed to be caused by the electric field of a long-wavelength, intense laser, and optical resonances are less important.[11,12] It can be called intense-laser field ionization (IFI). This technique is especially useful for studying the chemical dynamics in the case where a molecule passes through several electronically excited states that may appear dark in absorption.[10] In this work, this technique was used to study the early dynamics of $Cr(CO)_6$ dissociation after absorption of one UV photon at 267 nm in the gas phase. The ions produced by the delayed, intense probe laser pulse at 800 nm were detected by a time-of-flight mass spectrometer. Some features of one-color IFI of organometallics by femtosecond pulses were recently presented elsewhere.[13−15]

The energy levels relevant to dissociation and ionization of $Cr(CO)_6$ are presented in Figure 1.[16] The near-UV absorption

† On leave from B. I. Stepanov Institute of Physics, Belarus Academy of Sciences, Minsk, Belarus.

S1089-5639(97)03133-2 CCC: $15.00
Published on Web 02/18/1998

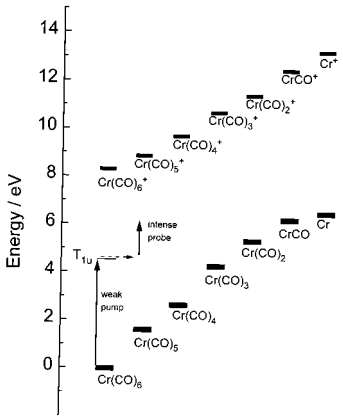

Figure 1. Energy balance for dissociation and ionization of $Cr(CO)_6$, based on compilation of experimental and theoretical data.[16] One pump photon of 4.65 eV excites the parent molecule into the metal-to-ligand charge-transfer state $^1T_{1u}$ (band origin at 4.43 eV). Its energy exceeds the values required to remove three CO ligands in the parent neutral molecule and five CO ligands in the parent ion molecule.

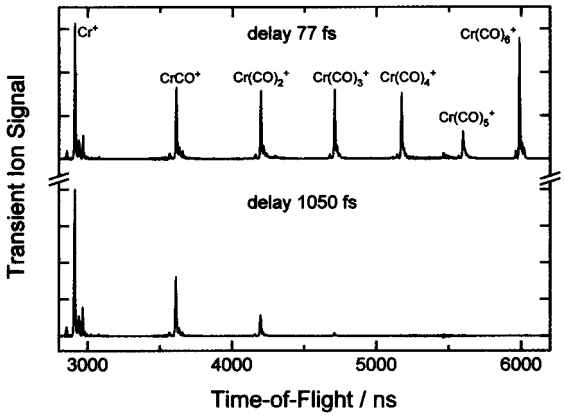

Figure 2. Transient time-of flight spectra obtained after irradiation of $Cr(CO)_6$ with pump pulses at 267 nm and delayed at 77- and 1050-fs probe pulses at 800 nm. The background due to ionization by probe pulses alone is subtracted.

spectrum of $Cr(CO)_6$ at photon energies of <5 eV is characterized by an intense $^1A_{1g} \rightarrow {}^1T_{1u}$ metal-to-ligand charge transfer (MLCT) transition at 4.43 eV and two weak shoulders at 3.60 and 3.91 eV,[21,22] which were recently reassigned to two of the forbidden singlet−singlet charge-transfer transitions, of which there are plenty in the 3.60−4.0 eV region.[23,24] Removal of three CO ligands is energetically possible after absorption of a single pump photon of 4.65 eV. Ionization of the parent molecule requires at least six probe photons of 1.55 eV.

In general, our results are consistent with a photochemical mechanism of chromium hexacarbonyl photodecomposition proposed by Burdett et al.[25] and give the real-time femtosecond dynamics of the process. The main features of this model are that electronically excited states of chromium pentacarbonyl are involved in the process and that geometrical distortion of it during internal conversion produces a vibrationally hot $Cr(CO)_5$ in the electronic ground state.

The paper is organized as follows. The experimental setup is briefly described in section 2. The results are presented in section 3. In section 4 we simulate the initial dynamics of the process by a rate-equation model and compare its results with the experimental data. We try to assign the levels of this model to real molecular states of the educt and product. In this section, we also discuss a conical intersection caused by the Jahn−Teller effect in chromium pentacarbonyl in a trigonal bipyramidal geometry. It provides a path for ultrafast internal conversion from the excited to the ground state.

2. Experimental Section

All experiments were conducted in the widely used pump−probe setup with a Ti:sapphire oscillator−amplifier system and a linear time-of-flight (TOF) mass spectrometer described elsewhere.[10,26,27] The measurements were made in the gas phase at room temperature. $Cr(CO)_6$ was excited near the origin of the MLCT transition $^1A_{1g} \rightarrow {}^1T_{1u}$ by 267-nm pulses with an energy of around 2 μJ. To probe the excited molecules, we used delayed 800-nm pulses with an energy of around 300 μJ and a full-width at half-maximum (fwhm) of 110 fs. The pump pulse duration was determined to be 130 fs fwhm by difference-frequency mixing with the 800-nm probe pulse in a 0.1-mm BBO crystal. The unfocused pump and focused (by a lens with a focal length of 50 cm) probe beams were collinearly combined and guided into the photoionization chamber. The peak probe-beam intensity in the focal plane was about 10^{13} W cm^{-2}, and the pump intensity was about 10^9 W cm^{-2}. The probe-beam polarization was set by a half-wave plate at an angle of 54.7° (magic angle) relative to the pump-beam polarization. Time zero was determined as the maximum of the transient ion signal for Xe, which is due to pure nonresonant (2 + 2) multiphoton ionization (MPI) under the given conditions. Two ion signals (normally a Xe peak and one of the Cr-containing signals) were recorded simultaneously by means of two boxcar integrators. This method provided synchronization of different scans with an accuracy of ±2 fs.

The $Cr(CO)_6$ (Fluka, 99%) and Xe (Linde, >99.9%) were introduced independently through two precision leak valves adjusted to produce in the ionization chamber pressures of the two gases of 10^{-7} and 10^{-5} mbar, respectively.

3. Experimental Results

At the pump wavelength of 267 nm, the intensities were less than 10^9 W cm^{-2}. Under these conditions the pump beam alone produced no measurable ion signal. The intensity of the probe beam was about 10^{13} W cm^{-2}, which is close to the threshold value for barrier-suppression ionization,[28] and the ionization mechanism under this condition is most likely nonresonant tunnel ionization.[29] Considering the energy balance, at least six photons of 800 nm are required to ionize the parent molecule. At the given intensities, the probe pulses alone produce noticeable ionization and around 84% of the ion yield appears in the form of parent ions.[30] The situation is very different when the pump precedes the probe pulse. Transient mass spectra obtained with probe pulses at 800 nm after pumping of $Cr(CO)_6$ at 267 nm are presented in Figure 2. The pump−probe delays were set at 77 and 1050 fs. For the first case the parent and all the metal-containing fragment ions $Cr(CO)_{n-1}^+$, $n = 6-1$, yielded similar intensities. With the longer delay, the ion signal is dominated by light fragments, of which the Cr^+ atomic ion contributes more than 30% and there are no parent and heavy fragment $Cr(CO)_n^+$, $n = 6-4$ ions.[31]

The measured transient ion signals of the parent molecule and of every fragment are shown in Figures 3 and 4. The three heaviest ions, $Cr(CO)_n^+$, $n = 6-4$, show an initial spike only and practically disappear after 300 fs. However, within this interval of 300 fs they do not coincide and their temporal behavior can be distinguished. Note that time zero was determined as the maximum of the transient ion signal for Xe, which is due to pure nonresonant (2 + 2) multiphoton ionization

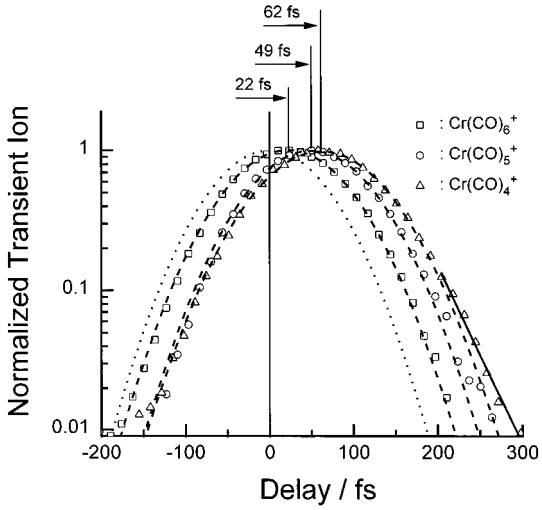

Figure 3. Semilog plot of the relative ion yield for the parent $Cr(CO)_6^+$ and fragment $Cr(CO)_5^+$ and $Cr(CO)_4^+$ ions vs the time delay between the 267-nm pump and the 800-nm probe. The symbols show the experimental data, and the dashed curves present the results of Gaussian fitting to the data. The solid line presents the results of single-exponential fitting to the $Cr(CO)_4^+$ ion tail, giving decay time constants of 34 ± 2 fs. The dotted curve is the response function calculated for a pump pulse of 130 fs fwhm and a probe pulse of 110 fs fwhm, on the assumption that three pump photons are used for ionization. The data are normalized to the maximum of the signal in each case.

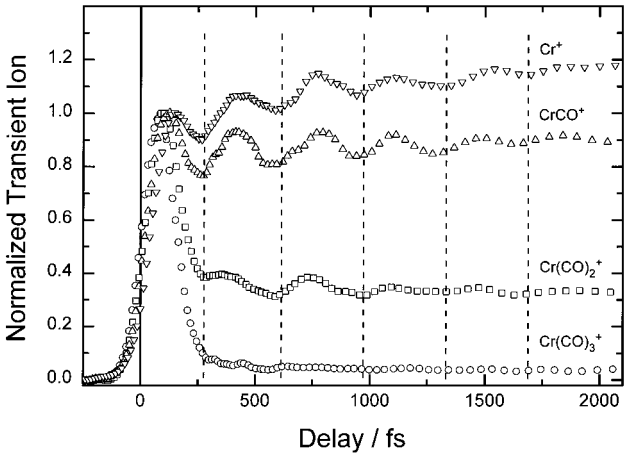

Figure 4. Plot of the relative ion yield for the fragment molecular $Cr(CO)_n^+$, $n = 3-1$, and atomic Cr^+ ions vs the time delay between the 267-nm pump and the 800-nm probe. Periodic modulation can easily be seen on the pedestal of light fragments. The data are normalized to the first peak of the signal in each case.

and should therefore give the absolute value of the zero point.[32] A response function was calculated for a pump pulse of 130 fs fwhm and a probe pulse of 110 fs fwhm on the assumption that three pump photons (which would yield the minimum energy required to ionize a parent molecule after an initial excitation) are used for the ionization (see dotted curve in Figure 3). This response function has a width of 145 fs (fwhm). The parent $Cr(CO)_6^+$ and the chromium pentacarbonyl $Cr(CO)_5^+$ ion signals show no asymmetry and fit well to a Gaussian function with 153 fs (fwhm). But their peaks are noticeably delayed by 22 and 49 fs, respectively. The chromium tetracarbonyl $Cr(CO)_4^+$ ion signal can also be reasonably well fitted by a 62-fs delayed Gaussian function with a width of 161 fs. However, some asymmetry in this signal can already be seen and single-exponential fitting to the $Cr(CO)_4^+$ ion tail in the region from 200 to 300 fs gives a decay time constant of 34 ± 2 fs.

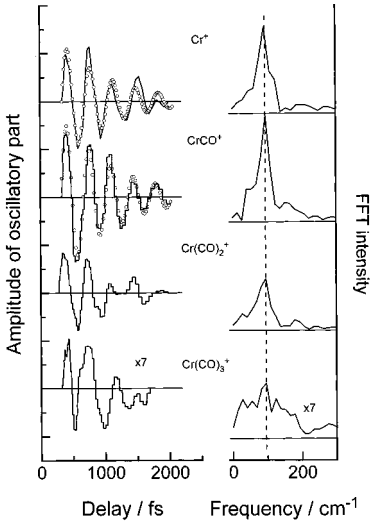

Figure 5. Oscillatory parts of ion signals along with their FT spectra for different fragments $Cr(CO)_n^+$, $n = 3-0$. The solid lines show the experimental data after subtracting a smooth background consisting of a low-order polynomial fit. The FT intensities of the oscillatory parts all peak at 96 cm^{-1} (marked by a dashed vertical line). The circles show a best fit of an exponentially decayed sine function (eq 1), which gives a time constant of 815 ± 20 fs for a coherence decay in Cr^+ and $CrCO^+$ signals.

Other molecular and atomic fragments $Cr(CO)_n^+$, $n = 3-0$, show a pedestal in addition to the initial spike (Figure 4). An obvious feature of all these pedestals is periodic modulation. Molecular ions $Cr(CO)_n^+$, $n = 3-1$, reach their peaks at 78-, 90-, and 125-fs delay, respectively (see also Figure 6). They then drop within less than 100 fs to average pedestal values of approximately 3.2, 33, and 90% of their respective maxima. The Cr^+ atomic ion, after a fast initial increase (the first peak is reached at 146 fs), shows minor secondary growth. Measurements on a longer time scale 0.2−300 ps (not shown in the figure) reveal biexponential growth of the atomic ion signal by approximately 30% with time constants of 0.93 ± 0.13 ps and 39 ± 6 ps. The initial part of this growth with superimposed modulation can be seen in Figure 4. Slow variations of the ion yield for $Cr(CO)_n^+$, $n = 3-1$, on a longer time scale 0.2−300 ps are less than 10% and deconvolution of any kinetic features is not sufficiently reliable with the present data.

To extract quantitative information on the oscillations mentioned above, the data were treated by discrete Fourier transform (FT) analysis. The oscillatory part of each ion signal in the region 0.3−2.2 ps, shown in Figure 5, is obtained by subtracting a smooth background consisting of a low-order polynomial fit. FT was taken over a 2.2-ps data range, yielding a spectral resolution of approximately 15 cm^{-1}. The FT window was started at 0.3 ps, excluding the time interval of the initial spike. The FT amplitudes of the oscillatory parts all peak at 96 cm^{-1}. Information about the decay of these coherent oscillations can be obtained by fitting the oscillatory parts Y_{coh} to the following exponentially damped sine function:[33]

$$Y_{coh} \propto \exp(-t/T_{coh.dec.}) \sin(2\pi t/T_{osc} + \phi) \qquad (1)$$

where $T_{coh.dec.}$ is the coherence decay time constant, T_{osc} the period of oscillation, and ϕ the relative phase. The best fit of function 1 to the less noisy Cr^+ and $CrCO^+$ signals gives $T_{coh.dec.} = 815 \pm 20$ fs. The results of this fit are shown by circles in Figure 5. It is remarkable that the coherence decay time constant is close to the fast secondary growth time constant of the Cr^+ signal of 930 ± 130 fs.

We did not measure the temporal behavior of the total ion (TI) yield, but it can easily be constructed from the kinetics of the parent and all the fragments (Figures 3 and 4) by using for normalization a TOF spectrum at a given time (Figure 2).[31] It is noteworthy that the TI signal has a peak at 70-fs delay, well separated from the maximum of the parent ion at 22 fs. The TI signal also shows secondary growth, just as the Cr^+ signal, and exhibits similar periodic modulation.

4. Simulation of the Kinetics and Discussion

4.1. Preliminary Considerations. The fact that at an early delay time of <300 fs every fragment shows different temporal behavior indicates that after initial excitation the molecule passes through several different configurations. The probability of formation of a specific fragment ion by the intense probe pulse changes with the configuration. Although the energy balance (Figure 1) shows that elimination of three CO ligands is possible after absorption of a single photon of 4.65 eV, a key point in interpreting the present experimental results is the assumption that *the primary photoproduct is vibrationally hot chromium pentacarbonyl in its electronic ground state*, which can be produced in a time interval as short as 300 fs after absorption of a single UV photon. This assumption is based on a comparison with the condensed-phase photochemistry of metal hexacarbonyls on a subpicosecond time scale. In solution and matrixes, single-photon photolysis eliminates only one CO ligand, regardless of the photon energy.[34] Femtosecond time-resolved UV−visible and UV−infrared transient-absorption measurements in solution reveal that $Cr(CO)_5$ is formed in its electronic ground state within 300 fs (see discussion in ref 2). Interaction with the solvent could produce some changes of the potential surfaces and the height of appropriate barriers (if any) and result in variation of the rate for unimolecular processes. But the change of the photochemical paths on this time scale is unlikely. Thus, we assume that the first CO is photochemically eliminated, leaving behind a hot $Cr(CO)_5$, and that in the gas phase the hot pentacarbonyl dissociates further, whereas in the condensed phase it cools instead. An additional justification for this assumption is an observation in a molecular beam: all dissociation products exhibited a statistical distribution, except the first CO, which showed nonstatistical behavior of the fragment internal and translational energies.[1]

4.2. Features of Ionization/Fragmentation by an Intense Laser Field. When considering the ionization/fragmentation pattern of electronically and/or vibrationally excited molecules that is caused by an intense laser pulse, we shall take into account the fact that there are three possible precursors to produce a specific metal-containing $Cr(CO)_n^+$ ion. First of all, it is worth remembering that any ion that is seen in our mass spectra should be cold enough so that it does not fragment within the extraction time of our TOF spectrometer (approximately 5 ns). Note also that there is a tendency for bond softening in the ion.[16] Therefore, one of the possible precursors for the $Cr(CO)_n^+$ ion is the neutral molecule $Cr(CO)_n$ in the ground or electronically excited state but with a vibrational energy below the threshold for dissociation of the ion. An example of this kind in our case is the transient formation of $Cr(CO)_6^+$ ions at an early time, which is obviously due to the ionization of initially electronically excited $Cr(CO)_6$. Ionization by an intense laser field can be considered as a vertical process in the sense that all the vibrational energy of the neutral precursor should be transferred to the ion. Therefore, if the neutral precursor $Cr(CO)_n$ has an internal vibrational energy exceeding the threshold for $Cr(CO)_n^+ \rightarrow Cr(CO)_{(n-k)}^+ + k$CO dissociation, upon ionization it will yield the light fragment $Cr(CO)_{(n-k)}^+$ only. The absence of $Cr(CO)_5^+$ and $Cr(CO)_4^+$ signals at delays longer than 300 fs can be explained by such a mechanism. A similar situation has also already been found in alkylbenzenes, where ionization from the vibrationally hot triplet state primarily produced fragment but not the parent ions.[35] Moreover, any ion can absorb additional photons from the tail of the intense laser pulse and exhibit further fragmentation. An obvious example of this process is the formation of the transient Cr^+ atomic ion, because the energy of a single pump photon is not sufficient to remove all the ligands, either from the parent neutral or from the parent ion.[16]

SCHEME 1: Rate-Equation Model for Simulation of the Initial Photochemical Decomposition of $Cr(CO)_6$

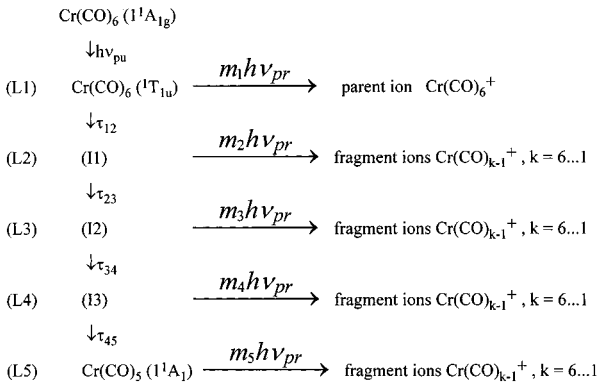

4.3. Simulation of the Kinetics of the Primary Photochemical Processes. To derive information about the dynamics of the primary photochemical decomposition of $Cr(CO)_6$ from the kinetics of the various ion signals, we employ a rate-equation model. The classical picture of femtosecond transition-state spectroscopy was previously successfully embraced by a kinetic model to describe the probing of a population during the different steps of the reaction.[36] Although the kinetic model ignores coherences, it is a powerful tool for providing insight into the population flow. A general scheme for calculating the ion signals convoluted with the real pulse shape of the pump and probe pulses has been discussed elsewhere.[10,27,36] Only features relevant to the process studied are considered here. It was found that the main features of the early kinetics for all ions can be reproduced by using the five-level rate-equation model depicted in Scheme 1 after convolution with the real pump and probe pulses.

In Scheme 1 the first level (L1) is the initially excited state $^1T_{1u}$ of the parent molecule $Cr(CO)_6$ and the fifth level (L5) is the primary photoproduct of the UV photodecomposition: the ground state 1^1A_1 of $Cr(CO)_5$. To account for the main features of the initial kinetics of all the fragments, we must introduce to Scheme 1 at least three intermediate levels: I1 = L2, I2 = L3, I3 = L4. In this scheme, the time constant τ_{ij} describes the lifetime of an *i*th level, which is determined by its decay to a subsequent *j*th level. The parameter m_i shows the order of the ionization process of the *i*th level used in the simulation. The results of the simulation are not very sensitive to the values of m_i in the range from 3 to 6, and for clarity we use the values m_i = 3, 3, 4, 5, 6 for $i = 1-5$, respectively. $m_{1(5)} = 3$ (6) reflects the minimum number of probe quanta required to ionize level L1 (L5). A set of parameters, for which the initial kinetics of all the ions within the five-level rate-equation model can be well simulated, is presented in Table 1. Figure 6 shows a comparison of the results of the simulation with the experimental data.

TABLE 1: Lifetimes τ_{ij} and Effective Ionization-Dissociation Cross Sections σ_{im} Used in the Five-Level Rate-Equation Model to Simulate the Initial Dynamics[a]

	level				
	L1 $\tau_{i,i+1} =$ 23 ± 1 fs	L2 $\tau_{i,i+1} =$ 10 ± 2 fs	L3 $\tau_{i,i+1} =$ 20 ± 2 fs	L4 $\tau_{i,i+1} =$ 40 ± 5 fs	L5 ∞
$Cr(CO)_6^+$	1.000	0	0	0	0
$Cr(CO)_5^+$	0	0.092	0.193	0	0
$Cr(CO)_4^+$	0	0	0.259	0.157	0
$Cr(CO)_3^+$	0	0	0.115	0.259	0.004
$Cr(CO)_2^+$	0	0	0.057	0.243	0.029
$CrCO^+$	0	0	0.062	0.160	0.080
Cr^+	0	0	0	0.280	0.207
Σ^+	1.000	0.092	0.686	1.100	0.320

[a] The values in rows 2−8 give the effective ionization-dissociation cross section σ_{im} to produce a specific ion m, indicated in the leftmost column from a given simulation level *i*, indicated in the first row. The cross sections are normalized in accordance with the transient mass spectrum at 77 fs (see Figure 2 and ref 31). The last row shows the total ionization cross section from the given *i*th level, which is the sum of the ionization-dissociation cross sections starting from the *i*th level and producing any fragment.

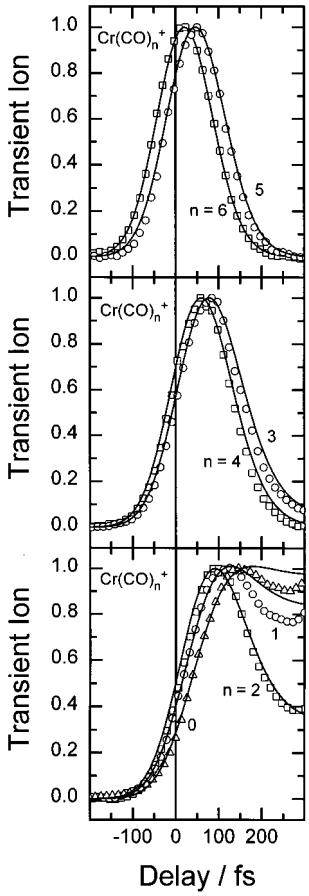

Figure 6. Comparison of the initial kinetics between normalized experimental data (symbols) and results of simulation (curves) within the five-level rate-equation model depicted by Scheme 1 with parameters presented in Table 1. Note that the simulation does not include coherent effects (coherent oscillations) and slow secondary thermal decomposition.

The main idea of the simulation is to have contributions only from a minimum number of precursor levels to each signal and to have a minimum number of levels in total. The results of the simulation show that both the shape and position of the parent ion signal can be well simulated by the contribution of the first level only with a lifetime $\tau_{12} = 23 \pm 1$ fs. The low uncertainty of ±1 fs of this value is mainly determined by the high sensitivity of the position of the simulated curve to the lifetime. It is also worth mentioning that a least-squares fit of the $Cr(CO)_6^+$ experimental data to a single exponential decay function convoluted with a Gaussian response function gives a width of the response function of 144.5 ± 0.5 fs (fwhm) and a decay time constant of 23.2 ± 0.2 fs. Note that the fitted width of the response function coincides well with the 145 fs deduced independently from the measured pump and probe pulse width and the assumption of a third-order ionization process from the first level L1 (see section 3). To reproduce the 27-fs delay of the $Cr(CO)_5^+$ signal in relation to the parent ion without noticeable broadening of the shape, we must introduce into the rate-equation model two short-lived intermediate levels I1 and I2 with lifetimes of 10 ± 2 and 20 ± 2 fs, respectively (Scheme 1). The third intermediate level I3 with a lifetime of 40 ± 5 fs describes both the delay and the slight asymmetry of the $Cr(CO)_4^+$ signal. Note that, to correctly reproduce the shape and delay of the fragment ion signals, we must assume at least two different levels of their neutral precursors for each signal (Table 1). The last row in Table 1 shows the total ionization cross section from the given *i*th level, which is the sum of the ionization-dissociation cross sections to produce any fragment from it. For further assignment it is important that the intermediate levels, I2 and I3, have ionization cross sections close to those of the initially excited state L1.

A comparison of the simulation with the experimental data is shown in Figure 6. It can be seen that both the shape and position of all seven observables are well reproduced. The slight deviation of the measured signal in the trailing edge of the Cr^+, $CrCO^+$, and $Cr(CO)_2^+$ is due to the coherent oscillations in the precursor level, L5 (ground state of neutral $Cr(CO)_5$), which were not taken into account. The quality of the fit for all of the different curves implies that the model has caught the essence of the underlying dynamics of the primary steps in the photodecomposition of $Cr(CO)_6$.

The calculation shows that 63% ($1 - e^{-1}$) of the population of the fifth level is produced within 110 fs. Since this level describes the primary photoproduct, ground-state $Cr(CO)_5$, this time can be denoted as the time to complete the primary step of the photochemical decomposition of $Cr(CO)_6$. The fact that this time is close to the period (76 fs) of a normal vibration on the reaction coordinate (Cr−C asymmetric stretch) implies that the dissociation proceeds almost directly within one oscillation period, although several different electronic states are involved in the process. This is discussed in the next section.

4.4. Vibrational Coherence and Pathway of the $Cr(CO)_6$ Photochemical Decomposition. In the delay interval 0.2−2 ps, where according to the foregoing discussion all ion signals are mainly due to ionization of one precursor, the primary photoproduct $Cr(CO)_5$ in its ground state, it is found that all the observable ionic fragments $Cr(CO)_n^+$, $n = 3-0$, and the total ion signal show pronounced modulation with a period of 350 fs, corresponding to a wavenumber of 96 cm^{-1}. Experimental information about the low-frequency vibrations of the unsaturated chromium pentacarbonyl is not available, but they are generally believed to be close to the corresponding vibrations of the parent molecule.[19,37] If so, the observed oscillation can be tentatively assigned to the $C_{ax}-Cr-C_{eq}$ bending vibration of the wavenumber 95 cm^{-1}. It is noteworthy that this vibration is not directly connected with the dissociation reaction coordinate, the Cr−C asymmetric stretch. Coherence in the photoproduct, first observed by Zewail and co-workers for the $HgI_2 \rightarrow HgI + I$ reaction,[38] is now commonly observed in the gas,

SCHEME 2: Primary Pathway of $M(CO)_6$ Photochemical Decomposition Proposed by Burdett et al.[25] (See Also Figure 7)

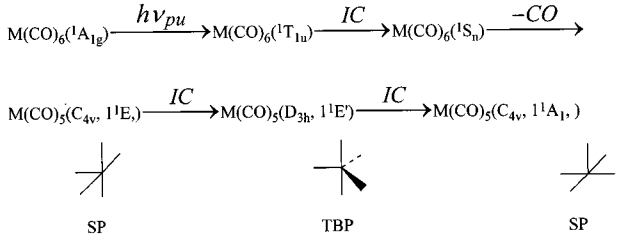

liquid, and solid phases. Although many features of this phenomenon have been documented and analyzed, a generalized picture of it is still under discussion. Bixon and Jortner recently presented an extensive list of papers devoted to experimental and theoretical studies of vibrational coherence effects in various molecular systems, ranging from small diatomic molecules to huge biophysical systems.[39] One aspect of coherent oscillations is the question of how the vibration is excited and in what way it produces an oscillating signal. To find the answer for our system, let us first consider the pathway and dynamics of the $Cr(CO)_6$ photodissociation.

On the basis of photolysis and spectroscopy of matrix-isolated metal hexa- and pentacarbonyl with polarized light and enlisting molecular-orbital considerations, Burdett et al.[25] proposed the mechanism for the primary dissociation of $Cr(CO)_6$ depicted in Scheme 2. It is also supported by quantum-chemical calculations.[40] In this mechanism, after the initial excitation to the MLCT state $^1T_{1u}$ centered at 4.43 eV, the parent molecule undergoes internal conversion (IC) to one of the lower singlet states ^1S_n, which are below 4 eV.[23] From this state the molecule dissociates, losing one CO to produce a square pyramid (SP) chromium pentacarbonyl of C_{4v} symmetry, which is assumed to be in the first excited singlet electronic state $M(CO)_5$ (C_{4v}, 1^1E) at an energy of around 2.0 eV. (Note that $Cr(CO)_5$ in equilibrium has a square pyramidal (SP) geometry with a droop angle $C_{ax}-Cr-C_{eq} = \Theta_{BPR}$ of about 93°.[41] Here, Θ_{BPR} is the doubly degenerate coordinate for the so-called Berry pseudorotation.) According to the Jahn−Teller theorem, the molecule is unstable in this degenerate excited state; the SP geometry will be distorted to a trigonal bipyramid (TBP) of D_{3h} symmetry with an equilibrium angle $C_{ax}-Cr-C_{eq}$ of 120°, and the molecule will then be in its lowest singlet state $^1E'$. (Note that the triplet ground state $^3A_2'$ of the TBP is situated about 0.6 eV lower than the $^1E'$ state, but the $^1A_1$ ground state in the SP geometry is even more stable by about 0.5 eV.[40]) Again, the electronic degeneracy will cause a Jahn−Teller instability so that the molecule can move downhill from the $^1E'$ state of the TBP along the same bending coordinate Θ_{BPR} and eventually reach the $^1A_1$ ground state of the SP. This mechanism, depicted in Scheme 2 and in greater detail in Figure 7, allowed Burdett et al.[25] to rationalize almost all their observations in the matrix photochemistry of $M(CO)_6$ and $M(CO)_5$. Further ultrafast time-resolved UV−visible and UV−infrared transient-absorption studies partly support this mechanism.[42,43] Nevertheless, no experimental results clearly giving the early-time dynamics of the photodissociation of transition-metal hexacarbonyls have yet been presented (see discussion in ref 2).

A simple comparison of our kinetic Scheme 1 with Burdett's photochemical Scheme 2 shows that the intermediate levels I1, I2, and I3, introduced to account for the temporal behavior of the fragment ions, can be assigned to the states $M(CO)_6$ (^1S_n), $M(CO)_5$ (C_{4v}, 1^1E), and $M(CO)_5$ (D_{3h}, $1^1E'$), respectively.

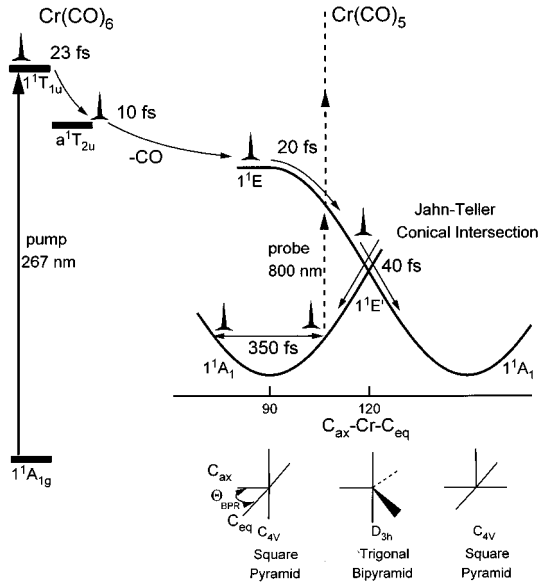

Figure 7. Schematic representation of early-time dynamics of UV photodecomposition of $Cr(CO)_6$. The energy-level scheme is based on the photochemical model suggested by Burdett et al.[25] and recent quantum-chemical calculations.[23,24] The time constants indicated are derived from simulation of all the ion kinetics with the five-level rate-equation model (see text).

Pierloot et al. report four additional singlet MLCT states below the bright $^1T_{1u}$, all of them involving $2t_{2g} \rightarrow 9t_{1u}$ (i.e., HOMO → LUMO) excitation and having strongly Cr−C antibonding character.[23] The lowest of them (a^1T_{2u}), with a calculated energy of 3.5−3.7 eV, is expected to be purely dissociative and to correlate with the singlet ground state 1^1E of SP.[24] To reach it, the $M(CO)_6$ (^1S_n) state should have at least 3.6 eV, as concluded from the energy balance of Scheme 2. So we suggest that $M(CO)_6$ (^1S_n) is just this, a^1T_{2u} state (or one of the similar states nearby). This would be in line with the philosophy that population redistribution among close-lying excited states is usually faster than the photochemical reaction. The absence of any contribution from this state in the parent-ion signal (see Table 1) indicates its significant displacement on the $Cr(CO)_5$−CO reaction coordinate and its repulsive character, which is also supported by its short lifetime of 10 fs. Note that the time for CO escaping is not 10 fs, but 33 = 23 + 10 fs, where 23 fs is the lifetime of the $^1T_{1u}$ state, since the parent molecule already starts to extend the Cr−CO distance on departure from the $^1T_{1u}$ state. The electronically excited character of the I2 and I3 intermediate states in Scheme 1 is also supported by their relatively high ionizability, which is comparable to the ionization probability of the initial excited-state $M(CO)_6$ ($^1T_{1u}$) (see Table 1). This high ionizability can be explained partly by the lowering of the ionization potential in $Cr(CO)_5$ in relation to the parent molecule and partly by assuming some intermediate resonances in the ionization process due to the denser electronic structure in chromium pentacarbonyl. In this context, it is also worth mentioning that an ultrafast (<100 fs) metal−ligand bond cleavage with formation of an unsaturated metal−carbonyl product in an electronically excited state was recently predicted by theoretical studies of metal carbonyl hydride photochemistry.[44] A similar ultrafast time scale for metal−ligand bond rupture has also been observed in $Mn_2(CO)_{10}$ and $Fe(CO)_5$ photodecomposition.[8,9]

Ultrafast motion between electronically excited states on a time scale comparable to a period of the reactive vibration is nowadays believed to be quite common in photochemistry.[45] On the other hand, nonadiabatic processes in which the molecule

moves from the excited- to the ground-state surface require special consideration. A long time ago, Teller suggested that an unavoided crossing at a conical intersection (CI) between two surfaces can provide conditions for effective radiationless decay within a single vibrational period.[46,47] Direct experimental confirmation of this mechanism was recently reported from this laboratory for a number of pericyclic photochemical reactions such as ring opening of 1,3-cyclohexadiene and hydrogen shift in 1,3,5-cycloheptatriene and its derivatives, where a lifetime of the lowest singlet state as short as 80 fs was measured.[10,27,48]

A true conical intersection is caused by the Jahn−Teller effect.[49] In this effect, a state degenerate in high symmetry splits by suitable nontotally symmetric deformations that themselves are often degenerate (as in the case of Θ_{BPR}). In this case, the potential surfaces near the point of degeneracy form a double cone in the space of the splitting coordinates. This situation is encountered twice in the dissociation product $Cr(CO)_5$: in the SP in the excited state 1^1E and in the TBP in the lowest singlet state $1^1E'$, with the same Jahn−Teller active coordinate Θ_{BPR}. (Only for the latter case is the conical intersection indicated in Figure 7.) These Jahn−Teller splittings are quantitatively given in detailed quantum-mechanical calculations of the lower singlet states of $Cr(CO)_5$ presented elsewhere.[25,40] The ultrafast departure (40 fs) from the lowest degenerate state of chromium pentacarbonyl to its ground state again confirms Teller's prediction[46] about the importance of conical intersections for efficient S_1/S_0 internal conversion.

This pathway also naturally explains the excitation of the observed coherent oscillations of the $C_{ax}-Cr-C_{eq}$ bending coordinate Θ_{BPR}. The molecule distorts on the way from the 1^1E state of SP to the $1^1E'$ state of TBP, changing the Θ_{BPR} angle from 90° to 120°, and then exhibits a reverse distortion to 90° in the ground state 1^1A_1 of the SP geometry. Upon this distortion, about 2 eV is released primarily to the $C_{ax}-Cr-C_{eq}$ bending vibration. However, the observed coherent oscillation has a frequency close to that of the normal vibration; i.e., it does not exhibit the properties of a high-amplitude vibration for which the frequency should be significantly lower as in the case of hindered rotations.[50] These oscillations also show no significant variation of the frequency within at least four periods, indicating no significant change of energy of these vibrations. Both facts allow us to conclude that a large fraction of the available energy is already channeled to different vibrations during the motion of the molecule from 1^1E to 1^1A_1 of SP via $1^1E'$ of TBP. It is worth emphasizing again that without involvement of an intermediate TBP geometry in the photochemical path, it would be difficult to explain the excitation of the observed coherent vibration along the Θ_{BPR} coordinate, since the equilibrium geometry of both the parent and primary products (SP chromium pentacarbonyl) have a Θ_{BPR} angle close to 90°! The observed coherent oscillations along the Θ_{BPR} coordinate represent a pure case of chemically induced vibrational coherence: the observed C−Cr−C bending vibrations are antisymmetric; they have a vanishing projection onto all (totally symmetric!) modes that are Franck−Condon active in the initial optical excitation of the transition $^1A_{1g} \rightarrow {}^1T_{1u}$ in $Cr(CO)_6$. This is in contrast to many other examples of coherent oscillations where coherence is already induced on the excited surface by superposition of Franck−Condon active modes by the ultrashort laser pulse.[39] It should also be pointed out that this oscillation would be difficult to explain if intersystem crossing was assumed, since the triplets do not present similar pathways between the geometries.

After clarifying how the coherent oscillations in ground-state $Cr(CO)_5$ are excited, we now consider the mechanism that visualizes them in the ionic signals $Cr(CO)_n^+$, $n = 3-0$. The 1^1A_1 state of the SP configuration has its maximum of absorption at around 2 eV, which is assigned to the $1^1A_1 \rightarrow 1^1E$ transition.[40] An increase of the Θ_{BPR} angle from the equilibrium value of 93° to 120° results in a decrease of the gap between these two states.[40] So one can expect a shift of the peak absorption to longer wavelengths at intermediate Θ_{BPR} values, providing conditions for one-photon resonance with the 1.55-eV probe photons used in our experiment. Moreover, since in ions all the hills are similar but generally lower, increasing Θ_{BPR} will also decrease the ionization potential and therefore increase the probability of intense-field ionization. Forward and backward oscillations along Θ_{BPR} in the ground state can therefore be expected to raise the ionization yield at some higher Θ_{BPR} values. Indeed, extrapolation of the oscillating curves (1) to the region of 0−300 fs shows that they have a maximum at a delay of 65 fs, indicating that the molecule appears on the ground-state surface at a geometry close to that for optimal ionization as expected from the above consideration.

On the ground-state surface, the primary photoproduct $Cr(CO)_5$ appears with a high vibrational energy of around 3 eV, which exceeds the energy of 2.47 eV, required to remove two more carbonyl ligands.[16] On the ground-state surface, chromium pentacarbonyl can be expected to exhibit thermal dissociation into $Cr(CO)_4$ and CO followed by further dissociation of at least part of $Cr(CO)_4$ to $Cr(CO)_3$ and CO. Note also that not all excess energy is available for dissociation, since some of it is removed by the released ligands.[51] Therefore, the two slower time constants of 0.93 and 39 ps observed in the small secondary growth of the Cr^+ signal can naturally be assigned to the thermal dissociation on the ground-state surface $Cr(CO)_5 \rightarrow Cr(CO)_4 + CO$ followed by partial further decomposition of $Cr(CO)_4$ to $Cr(CO)_3 + CO$. (Note that, owing to their energy distribution, not all of the $Cr(CO)_4$ molecules can dissociate.) The more pronounced secondary growth of the Cr^+ signal compared with the molecular fragments $Cr(CO)_n^+$, $n = 3-1$, can be explained by the increasing probability that the photodissociation of hot ions would produce lighter fragments such as Cr^+. It is worth mentioning that RRKM calculations predict statistical rates for thermal dissociation of $Cr(CO)_5$ exceeding 10^{12} s^{-1} at internal energies higher than 3.6 eV and for thermal dissociation of $Cr(CO)_4$ greater than 2.5×10^{10} s^{-1} at energies greater than 2.2 eV.[5] This is in reasonable agreement with the experimental results and confirms our assignment. The coincidence of the faster thermal dissociation time constant with a time constant for loss of coherence implies that the damping of the vibrational coherence is mainly due to decomposition of the precursor but not due to vibrational dephasing.

It is also interesting to discuss the apparent difference between our data and the results of experiments on non-time-resolved low-energy electron-impact ionization probing after nanosecond pulse excitation at 248 nm.[1,52] In that case, $Cr(CO)_4^+$ was observed to be the dominant one-photon photofragment, while in our experiment the $Cr(CO)_4^+$ signal already disappears after 200 fs. In our opinion, this apparent difference is most likely connected with the ionization mechanism by the probe. After thermal decomposition of the vibrationally hot primary photoproduct $Cr(CO)_5$, chromium tetracarbonyl is produced with an internal energy of 1.3−1.9 eV. Ionization by an intense laser field is an instantaneous, purely vertical process where all of the vibrational energy of a neutral precursor is transferred to the ion. The dissociation threshold for $Cr(CO)_4$ is 0.6 eV for

the ion versus 1.4 eV for the neutral.[16] Consequently, the ion excess energy is well above the dissociation threshold and the ion will exhibit fragmentation. So in the mass spectrum only stable ion fragments with low internal energy can be seen. In our case at longer delay this means $Cr(CO)_n^+$, $n = 3-0$. Ionization by low-energy electron impact proceeds via formation of an intermediate anion complex with a lifetime long enough for redistribution of internal energy and nonvertical processes to become possible. Hence, fragmentation is reduced in relation to vertical ionization (by photons or fast electrons). In the given case, the neutral precursor is mainly $Cr(CO)_4$ and to a small extent also $Cr(CO)_3$.

5. Conclusions

Direct probing of gas-phase, single-UV-photon photolysis of $Cr(CO)_6$ by femtosecond-pump ionization-probe spectroscopy with time-of-flight detection of the parent and all the fragment ions reveals an intricate series of elementary events that together comprise the full course of decarbonylation in this molecule. Our results are consistent with the photochemical mechanism of $Cr(CO)_6$ photodecomposition proposed by Burdett et al.[25] and give the following real-time dynamics of the process (see also Figure 7): (1) In the initially excited MLCT $^1T_{1u}$ state the $Cr(CO)_6$ molecule lives 23 fs and then drops to the lowest excited singlet state of $Cr(CO)_6$ a^1T_{2u} or another low excited singlet state; (2) from the a^1T_{2u} state the molecule dissociates, losing one CO ligand with a time constant of 10 fs, and arrives at the lowest excited state 1^1E of $Cr(CO)_5$ in square-pyramid (SP) geometry; (3) from the SP 1^1E state, the $Cr(CO)_5$ molecule is distorted along the $C_{ax}-Cr-C_{eq}$ bending coordinate Θ_{BPR} (Berry pseudorotation) and drops within 20 fs to the lowest excited singlet state of trigonal-bipyramid (TBP) geometry $1^1E'$;- from the TBP $1^1E'$ state the $Cr(CO)_5$ molecule is again distorted along Θ_{BPR} and drops within 40 fs via a Jahn−Teller induced conical intersection to the ground state $^1A_1$, which is of SP geometry; (4) the initial photodissociation is complete within 100 fs; (5) on the $^1A_1$ surface, the primary photoproduct $Cr(CO)_5$ exhibits a coherent oscillation on the Θ_{BPR} coordinate, which is damped by thermal decomposition of $Cr(CO)_5$ within approximately 900 fs.

Other group VI transition-metal (Mo, W) hexacarbonyls have very similar electronic spectroscopy and geometrical structure, and so one can also expect similar early-time dynamics of their UV photodecomposition. More experiments using femtosecond lasers at different wavelengths are under preparation to provide additional information about early-time photodissociation dynamics of chromium and other transition-metal hexacarbonyls.

Acknowledgment. The authors thank T. Schikarski for his valuable help in the experiment and W. Ritt for his skillful technical assistance.

References and Notes

(1) Venkataraman, B.; Hou, H.; Zhang, Z.; Chen, S.; Bandukwalla, G.; Vernon, M. *J. Chem. Phys.* **1990**, *92*, 5338 and references therein.

(2) Lian, T.; Bromberg, S. E.; Asplund, M. C.; Yang, H.; Harris, C. B. *J. Phys. Chem.* **1996**, *100*, 11994 and references therein.

(3) Jackson, R. L. *Acc. Chem. Res.* **1992**, *25*, 581 and references therein.

(4) Trushin, S. A.; Sugawara, K.; Takeo, H. *Chem. Phys. Lett.* **1995**, *236*, 402.

(5) Trushin, S. A.; Sugawara, K.; Takeo, H. *Chem. Phys.* **1996**, *203*, 267.

(6) Rayner, D. M.; Ishikawa, Y.; Brown, C. E.; Hackett, P. A. *J. Chem. Phys.* **1991**, *94*, 5471.

(7) Zewail, A. H. *Femtochemistry: Ultrafast Dynamics of the Chemical Bond*; World Scientific: Singapore, 1994; Vols I and II and references therein.

(8) Kim, S. K.; Pedersen, S.; Zewail, A. H. *Chem. Phys. Lett.* **1995**, *233*, 500.

(9) Banares, L.; Baumert, T.; Bergt, M.; Kiefer, B.; Gerber, G. *Chem. Phys. Lett.* **1997**, *267*, 141. Banares, L.; Baumert, T.; Bergt, M.; Kiefer, B.; Gerber, G. *J. Chem. Phys.*, in press.

(10) Trushin, S. A.; Fuss, W.; Schikarski, T.; Schmid, W. E.; Kompa, K. L. *J. Chem. Phys.* **1997**, *106*, 9386.

(11) Augst, S.; Meyerhofer, D. D.; Strickland, D.; Chin, S. L. *J. Opt. Soc. Am. B* **1991**, *8*, 858.

(12) Dewitt, M. J.; Levis, R. J. *J. Chem. Phys.* **1995**, *102*, 8670.

(13) Grun, C.; Weickhardt, C.; Grotemeyer, J. *Eur. Mass Specrom.* **1995**, *2*, 197.

(14) Willey, K. F.; Brummel, C. L.; Winograd, N. *Chem. Phys. Lett.* **1997**, *267*, 359.

(15) Lindener, J.; Grossekathoefer, M.; Janello, J.; Dickebohm, M. S.; Gutmann, M. In *The 3rd Conference on Femtochemistry*, August 31 through September 4, 1997, Lund, Sweden; Book of Abstracts; Lund University: Sweden, 1997; p 45; a work submitted to a special issue of *J. Phys. Chem.* on femtochemistry.

(16) The bond dissociation energies (BDE) $Cr(CO)_{n-1}-CO$ in neutral molecules at 298 K are considered to be 1.60, 1.08, 1.39, 1.23, 1.23, and 0.06 eV, for $n = 6-1$, respectively,[1,17,18] and in ions, 1.40, 0.66, 0.59, 0.59, 0.98, 0.95 eV, respectively.[19] Using ionization energies for $Cr(CO)_6$ and Cr of, respectively, 8.19 and 6.766 eV[19,20] and the above values for the BDEs, one can calculate ionization potentials for $Cr(CO)_{n-1}$ ($n = 6-2$) of 8.02, 7.58, 6.72, 6.1, 5.89, respectively.

(17) Fletcher, T. R.; Rosenfeld, R. N. *J. Am. Chem. Soc.* **1988**, *110*, 2097.

(18) Trushin, S. A.; Sugawara, K.; Takeo, H. *Chem. Phys. Lett.* **1997**, *267*, 573.

(19) Khan, F. A.; Clemmer, D. E.; Schultz, R. H.; Armentrout, P. B. *J. Phys. Chem.* **1993**, *97*, 7978.

(20) Sugar, J.; Corliss, C. *J. Phys. Chem. Ref. Data* **1977**, *6*, 317.

(21) Beach, N. A.; Gray, H. B. *J. Am. Chem. Soc.* **1968**, *90*, 5713.

(22) Kotzian, M.; Rösch, N.; Schröder, H.; Zerner, M. C. *J. Am. Chem. Soc.* **1989**, *111*, 7687.

(23) Pierloot, K.; Tsokos, E.; Vanquickenborne, L. G. *J. Phys. Chem.* **1996**, *100*, 16545.

(24) Pollak, C.; Rosa, A.; Baerends, E. J. *J. Am. Chem. Soc.* **1997**, *119*, 7324.

(25) Burdett, J. K.; Grzybowski, J. M.; Perutz, R. N.; Poliakoff, M.; Turner, J. J.; Turner, R. F. *Inorg. Chem.* **1978**, *17*, 147.

(26) Fuss, W.; Schikarski, T.; Schmid, W. E.; Trushin, S. A.; Kompa, K. L. *Chem. Phys. Lett.* **1996**, *262*, 675.

(27) Fuss, W.; Schikarski, T.; Schmid, W. E.; Kompa, K. L.; Trushin, S. A. Manuscript in preparation.

(28) The threshold intensity for ionization by barrier suppression is 1.8×10^{13} W cm^{-2}, as calculated by using formula 6 from ref 11 for the ionization potential of 8.19 eV.

(29) Ledingham, K. W. D.; Singhal, R. P. *Int. J. Mass Spectrom. Ion Processes* **1997**, *163*, 149 and references therein.

(30) The distribution of the ion yield $Cr(CO)_n^+$ ($n = 6-0$) with ionization by 800 nm alone is 84:0.5:0.8:1.1:1.7:4.2:7.7%, respectively.

(31) The distribution of the transient ion yield $Cr(CO)_n^+$ ($n = 6-0$) with 77- and 1050-fs delay (see Figure 2) is 18.0:7.3:12.3:13.0:13.0:14.0: 22.4% and 0:0:0:1.2:9.3:25.0:64.5%, respectively.

(32) Fisher, I.; Vrakking, M. J. J.; Villeneuve, D. M.; Stolow, A. *Chem. Phys.* **1996**, *207*, 331.

(33) Szarka, A. Z.; Pugliano, N.; Palit, D. K.; Hochstrasser, R. M. *Chem. Phys. Lett.* **1995**, *240*, 25.

(34) Geoffroy, G. L.; Wrighton, M. S. *Organometallic Photochemistry*; Academic: New York, 1979.

(35) Duncan, M. A.; Dietz, T. G.; Smalley, R. E. *J. Chem. Phys.* **1981**, *75*, 2118. Dietz, T. G.; Duncan, M. A.; Smalley, R. E. *J. Chem. Phys.* **1981**, *76*, 1227.

(36) Pedersen, S.; Zewail, A. H. *Mol. Phys.* **1996**, *89*, 1455 and references therein.

(37) Jonas, V.; Thiel, W. *J. Chem. Phys.* **1995**, *102*, 8474.

(38) Dantus, M.; Bowman, R. M.; Gruebele, M.; Zewail, A. H. *J. Chem. Phys.* **1989**, *91*, 7437.

(39) Bixon, M.; Jortner J. *J. Chem. Phys.* **1997**, *107*, 1470 and references therein.

(40) Hay, P. J. *J. Am. Chem. Soc.* **1978**, *100*, 2411.

(41) Barnes, L. A.; Liu, B.; Lindh, R. *J. Chem. Phys.* **1993**, *98*, 3978.

(42) Joly, A. J.; Nelson, K. A. *J. Phys. Chem.* **1989**, *93*, 2876.

(43) Wang, L.; Zhu, X.; Spears, K. G. *J. Am. Chem. Soc.* **1988**, *110*, 8696.

(44) Daniel, C.; Kolba, E.; Lehr, L.; Manz, J.; Schroder, T. *J. Phys. Chem.* **1994**, *98*, 9823. Heitz, M.; Daniel, C. *J. Am. Chem. Soc.* **1997**, *119*, 8269.

(45) Fuss, W.; Hering, P.; Kompa, K. L.; Lochbrunner, S.; Schikarski, T.; Schmid, W. E.; Trushin, S. A. *Ber. Bunsen-Ges. Phys. Chem.* **1997**, *101*, 500.

(46) Teller, E. *J. Phys. Chem.* **1937**, *41*, 109. Teller, E. *Isr. J. Chem.* **1969**, *7*, 227.

(47) Bernardi, F.; Olivucci, M.; Robb, M. A. *Chem. Soc. Rev.* **1996**, *25*, 321.

(48) Fuss, W.; Kompa, K. L.; Lochbrunner, S.; Müller, A. M. S.; Schikarski, T.; Schmid, W. E.; Trushin, S. A. In *The 3rd Conference on Femtochemistry*, August 31 through September 4, 1997, Lund, Sweden; Book of Abstracts: Lund University: Sweden, 1997; p 21.

(49) Herzberg, G. *Molecular Spectra and Molecular Structure: III. Electronic Spectra and Electronic Structure of Polyatomic Molecules*; Van Nostrand: Princeton, 1966; Chapter 3.

(50) Lister, D. G.; MacDonald, J. N.; Owen, N. L. *Internal Rotation and Inversion, an Introduction to Large Amplitude Motion in Molecules*; Academic Press: London, 1978.

(51) Fletcher, T. R.; Rosenfeld, R. N. *J. Am. Chem. Soc.* **1985**, *107*, 2203.

(52) Tyndall, G. W.; Jackson, R. L. *J. Chem. Phys.* **1989**, *91*, 2881.